# The High Power Impulse Magnetron Sputtering Discharge: The Ionization Mechanism

J.T. Gudmundsson, Science Institute and Department of
Electrical and Computer Engineering, University of Iceland, Reykjavik, Iceland

## ABSTRACT

The high power impulse magnetron sputtering (HIPIMS) is a promising addition to existing physical vapor deposition (PVD) techniques. It provides high plasma densities and high fractional ionization of the sputtered material. Here, the ionization mechanism and the temporal behavior of the plasma parameters in a high power impulse magnetron sputtering discharge are investigated using a time dependent global (volume averaged) model. The ionized metal fraction and the ionized flux fraction are very high and the integrated ionized flux fraction is 0.89 for aluminum. During the pulse on period electron impact ionization is the most effective mechanism in creating metal ions while charge exchange becomes the dominant mechanism in creating metal ions after the pulse is off.

## INTRODUCTION

The magnetron sputtering discharge has found widespread use in various coating processes including hard, wear-resistant coatings, low friction coatings, corrosion resistant coatings, decorative coatings and coatings with specific optical or electrical properties. In a conventional dc magnetron sputtering discharge only a small fraction of the sputtered atoms are ionized, roughly on the order of 1%. Recently magnetron sputtering discharges have been developed that can generate highly ionized plasma most commonly by adding a secondary discharge between the cathode target and the substrate. An alternative is the method referred to as high power impulse magnetron sputtering (HIPIMS) which was introduced over a decade ago [1] and later shown to give high degree of ionization of the sputtered material [2,3]. A brief review of the technique and its application has been given by Helmersson et al. [4,5].

HIPIMS has the advantage of using essentially the conventional magnetron sputtering equipment except for the power supply. For conventional dc magnetron sputtering, the maximum power is limited by the thermal load on the target provided by bombardment of the positive ions. To avoid this limitation, the power may be applied in pulses. By decreasing the duty cycle (on-time divided by the cycle-time), a corresponding increase in power during the on-time can be achieved. The power supply for a high power pulsed magnetron sputtering are usually based on an artificial pulse-forming network and consist of a single or multiple mesh *LC* networks as seen in Figure 1. These systems operate in a repetitively pulsed manner. The pulse generator consist of a discharge capacitor which is connected to be charged from a charging circuit through a thyristor switch. The capacitor $C_s$ is then discharged over the electrodes of the sputtering device through an inductor $L$. The inductance coil is connected in series with the magnetron discharge in order to reduce the rate of current rise. The pulse length is typically 50 - 500 $\mu$s and the pulse frequency 1 – 500 Hz. The high power pulse has a peak cathode voltage in the range 500 – 2000 V which gives peak power densities in the range 1 - 3 kW/cm$^2$ [6,7]. The exact pulse shape is determined by the load, the discharge formed in the sputtering device, and depends thus on the gas type and gas pressure. This is seen in Figure 2 where the shape of the power pulse depends on the discharge gas pressure. The actual pulse-width decreases with increasing discharge gas pressure.

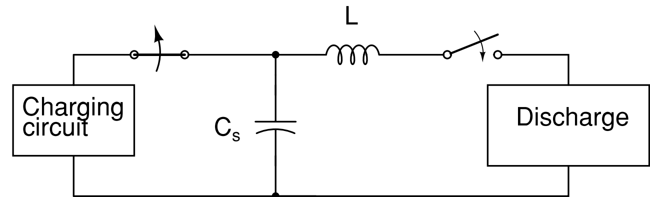


Figure 1: The basic single mesh LC network between the charging power supply and the discharge load.

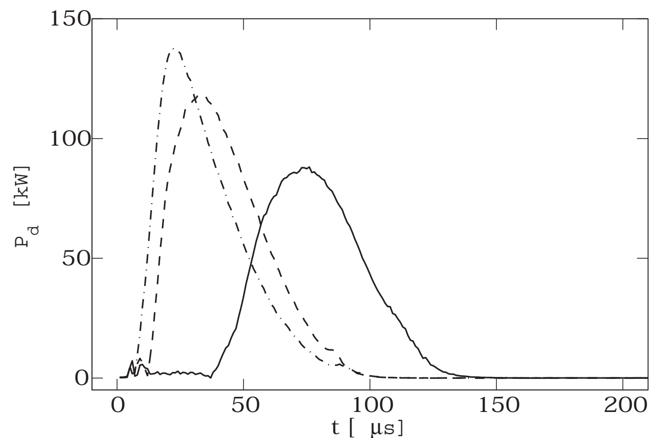


Figure 2: The power applied to the discharge versus time from the pulse initiation. The target was made of tantalum 150 mm in diameter, and the argon gas pressure was 0.5 mTorr (solid line), 2 mTorr (dashed line) and 10 mTorr (dot dashed line).

© 2006 Society of Vacuum Coaters 505/856-7188

49th Annual Technical Conference Proceedings (2006) ISSN 0737-5921

When the flux of ions is higher than the flux of neutrals or $\Gamma_{m+} > \Gamma_m$ the process is referred to as ionized physical vapor deposition (IPVD) [8]. The development of IPVD techniques was initially driven by the need to deposit metal layers and diffusion barriers into trenches or vias of high aspect ratio IC structures [9], but has during the past years found a number of additional applications. The ions are preferred since their energy and direction can be controlled. Thus, ionizing the sputtered vapor has several advantages including enhanced step coverage and improvement of the film quality, such as density and adhesion, especially for substrates of complex shape.

HIPIMS has been successfully developed to produce high plasma densities of the order of $10^{19}$ $m^{-3}$ [2,10-12] and to obtain highly ionized metal plasmas [6,13]. A high fractional ionization has been demonstrated and values higher than 90% at pulse energy of 2 J for Ti target have been reported [13]. Measurements of the ionized flux fraction have also been made using weight gain differences on a floating and a positively biased substrate. This way, the ionized flux fraction for Cu and Cr has been estimated to be roughly 70% [2] and 30% [14], respectively. The degree of metal ionization of the flux from a $Ti_{0.5}Al_{0.5}$-target has been reported to be around 40% [3]. Using a quartz crystal microbalance (QCM) the degree of ionization of C and Al during sputtering was measured to be 4.5% and 9.5%, respectively [15]. These values are significantly lower than those reported by the other groups. For C, a lower ionization fraction is expected since it has a higher ionization potential and a smaller electron impact cross section as compared to metals where the obtained ion fractions are relatively high.

The reported ionized flux fraction for metals range from about 10% to over 80%. The reported values are highly inconsistent which may be related to various magnetron configuration and/or applied power density. Here we explore the ionization mechanism and the temporal behavior of the plasma parameters in a high power pulsed magnetron sputtering discharge and estimate the fractional ionization

## MODEL OF THE IONIZATION MECHANISM

To explore the plasma parameters and the ionization mechanism for highly ionized magnetron sputtering a simple time dependent global model was developed, based on the time dependent global model for argon discharge [16] and extended to include metal species as described by Hopwood and Qian [9,17]. The discharge is assumed to consist of electrons, Ar atoms in the ground state, metastable argon atoms $Ar^*$, $Ar^+$ ions, metal atoms M, and metal ions, $M^+$. Electrons are assumed to have a Maxwellian energy distribution in the range 1-7 eV. The reactions and rate coefficients assumed in the model are listed in Table 1. The plasma chemistry is described by a set of first-order differential equations. For each species a continuity equation describes the creation and the volumetric and surface reactions and losses.

Table 1: The reactions used to construct a global (volume averaged) model of the HIPIMS discharge.

| Reaction | $k$ [m$^3$/s] | Ref. |
|---|---|---|
| $e + Ar \longrightarrow Ar^+ + 2e$ | $k_{iz}$ | [20] |
| $e + Ar \longrightarrow Ar^* + e$ | $k_{exc}$ | [21] |
| $e + Ar^* \longrightarrow Ar^+ + 2e$ | $k_{exc,iz}$ | [22] |
| $e + Ar^* \longrightarrow Ar + e$ | $k_{deexc} = 4.3 \times 10^{-16} T_e^{0.74}$ | [16] |
| $Ar^+ \longrightarrow Ar(wall)$ | $k_{wall,Ar+} = 2u_B(h_L R^2 + h_R RL)/R^2 L$ | |
| $Ar^* \longrightarrow Ar(wall)$ | $D_{Ar}\left[\left(\frac{\pi}{L}\right)^2 + \left(\frac{2.405}{R}\right)^2\right]$ | |
| $e + Al \longrightarrow Al^+ + 2e$ | $k_{izm} = 1.23 \times 10^{-13} \exp(-7.23/T_e)$ | [9] |
| $Al^+ \longrightarrow Al(wall)$ | $k_{wall,Ar+} = 2u_B(h_L R^2 + h_R RL)/R^2 L$ | |
| $Al \longrightarrow Al(wall)$ | $D_m\left[\left(\frac{\pi}{L}\right)^2 + \left(\frac{2.405}{R}\right)^2\right]$ | |
| $Ar^* + Al \longrightarrow Al^+ + Ar + e$ | $k_P = 5.9 \times 10^{-16}$ | [23] |
| $Ar^+ + Al \longrightarrow Al^+ + Ar$ | $k_{chex} = 1 \times 10^{-15}$ | [23] |

The power balance equation, which equates the absorbed power $P_{abs}$ to power losses due to elastic and inelastic collisions and losses due to charged particle flow to walls is given as

$$\frac{d}{dt}\left(\frac{3}{2}en_eT_e\right) = \frac{P_{abs}}{V} - e\mathcal{E}_c k_{iz} n_{Ar} n_e - e k_{wall,Ar^+}(\mathcal{E}_e + \mathcal{E}_i) n_{Ar^+} \quad (1)$$

where $n_e$ is the electron density, $T_e$ is the electron temperature, $n_{Ar}$ is the neutral argon density, $n_{Ar+}$ is the density of argon ions, $\varepsilon_e$ is the mean kinetic energy per electron lost and $\varepsilon_i$ is the mean kinetic energy per ion lost and $k_{wall,Ar+}$ accounts for the flux of $Ar^+$ ions to the chamber walls and is given in Table 1. Here $\varepsilon_c$ is the collisional energy loss per electron-ion pair created and is defined as

$$\mathcal{E}_c = \mathcal{E}_{iz} + \sum_i \mathcal{E}_{ex,i}\frac{k_{ex,i}}{k_{iz}} + \frac{k_{el}}{k_{iz}}\frac{3m_e}{m_i}T_e \quad (2)$$

where $\varepsilon_{iz}$ is the ionization energy, $\varepsilon_{ex,i}$ is the threshold energy for the $i$-th excitation process, $k_{iz}$ is the ionization rate coefficient, $k_{ex,i}$ is the rate coefficient for the $i$-th excited state and $k_{el}$ is the elastic rate coefficient (see [18]). The ratios of the density at the sheath edge to that in the bulk for the axial and radial directions are $h_L = 0.86\ [3+ L/2\lambda_i]^{-1/2}$ and $h_R = 0.80\ [4+ R/\lambda_i]^{-1/2}$, respectively [19]. Here, $\lambda_i = n_{Ar}\sigma_i$ is the ion-neutral mean free path and $\sigma_i$ is the ion-neutral scattering cross section. The combined ionic momentum transfer cross section for these two processes is roughly $10^{-18}$ $m^2$ for the thermal energies of interest.

We assume that metal ions are generated by electron impact ionization $e+M \rightarrow M^+ +2e$ with a rate coefficient $k_{miz}$, by Penning ionization, collision with an electronically excited argon atom $Ar^* + M \rightarrow M^+ + Ar + 2e$ with a rate coefficient $k_P$ and by charge exchange $Ar^+ + M \rightarrow M^+ + Ar$ with a rate coefficient $k_{chexc}$. The metal ions are assumed to be lost to solid surfaces such

as the chamber walls described by $k_{wall,m+}$. From the reaction set listed in Table 1 a particle balance equation for the metal ions is created.

The metal atoms enter the plasma as they are sputtered from the cathode target. The reaction rate for the metal atoms as they are sputtered from the target is $\Upsilon_{sput} h_L u_B r_T^2/(R^2 L) n_{Ar+}$ where $\Upsilon_{sput}$ is the yield of sputtered atoms per incident ion, $r_T$ is the target radius and $u_B=(eT_e/m_i)^{1/2}$ is the Bohm velocity, $n_{Ar+}$ is the argon ion density, and $m_i$ is the argon ion mass. The loss of metal atoms includes electron impact ionization with rate coefficient $k_{miz}$, Penning ionization and charge exchange with argon ions with rate coefficient $k_{chexc}$, and the diffusion loss of metal atoms given by $D_m/\Lambda^2$ where $\Lambda$ is effective diffusion length of neutral species and the metal atom diffusion coefficient is $D_m=eT_g\Lambda/m_m v_{th}$ where $v_{th}=(8eT_g/\pi m_m)^{1/2}$ is the mean neutral speed and $m_m$ is the metal atom mass. A particle balance equation for metal atoms is created using the reactions listed in Table 1.

The reaction rate for Penning ionization depends on the density of the metastable argon atoms which are produced by electron impact excitation $e+Ar \rightarrow Ar^*+e$ with rate coefficient $k_{exc}$ and are lost by Penning ionization, electron impact deexcitation with a rate coefficient $k_{deexc}$, electron impact ionization $e+Ar^* \rightarrow Ar^+ + e$ with rate coefficient $k_{exc,iz}$ and diffusion of metastable argon atoms to the chamber walls. A particle balance equation for generation and loss of metastable argon is constructed from the reaction set listed in Table 1.

The argon ions are created by electron impact ionization from argon atoms in ground and metastable states with rate coefficients $k_{iz}$ and $k_{exc,iz}$, respectively. They are lost by charge exchange with metal atoms and as flux to the chamber walls. The particle balance for argon ions is constructed from the reaction set listed in Table 1.

The temporal variation of the particle density and the electron temperature was obtained by solving the five differential equations, the power balance (equation (1)), the particle balance for metal ions, the particle balance for metal atoms, the particle balance for argon ions and the particle balance for metastable argon atoms simultaneously and self-consistently. Once the density of $Ar^+$ and $M^+$ is found the quasi-neutrality condition gives the electron density $n_e = n_{Ar+} + n_{m+}$.

## RESULTS AND DISCUSSION

To explore the ionization processes in a high power impulse magnetron sputtering discharge we assume a discharge chamber of radius $R$=15 cm and length $L$=15 cm with a target of radius $r_T$=7.5 cm made of aluminum. The plasma chamber geometry is an important parameter in controlling the discharge processes. As the chamber dimensions increase the rate at which ions are lost to the walls decreases. To compensate for decreased loss the electron temperature decreases. We assume the power pulse to be the same as shown in Figure 2 and the discharge pressure to be 10 mTorr. The reaction set used is listed in Table 1 and the electron energy distribution is assumed to be Maxwellian. We assume the sputtering yield for argon ion bombardment of aluminum at 1000 eV to be $\Upsilon_{sput}$=2 [24]. Figure 3 shows the electron density, argon ion density, the aluminum ion density and the aluminum atom density versus time from the pulse initiation. The argon ion density increases sharply when the pulse is initiated and peaks at $3\times10^{19}$ $m^{-3}$ 53 $\mu$s after initiating the pulse. The argon ion density then decays. The applied power peaks at 137 kW 22 $\mu$s after initiating the pulse. The aluminum ion density peaks at $2\times10^{18}$ $m^{-3}$ 99 $\mu$s after initiating the pulse. The aluminum atom density peaks at $7\times10^{17}$ $m^{-3}$ 148 $\mu$s after initiating the pulse. The argon ion density is always higher than the aluminum ion density. The first 2 ms of the discharge the aluminum ion density dominates the aluminum atom density. The temporal behavior of the electron temperature is shown in Figure 4. A sharp spike is shown in the electron temperature at the pulse initiation. Then a broader peak of 4.55 eV appears 12 µs after initiating the pulse. 300 µs into the pulse the electron temperature is below 0.1 eV.

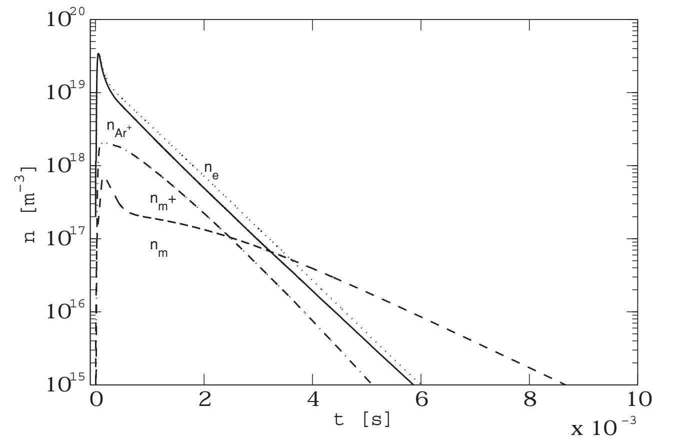


Figure 3: The electron density, argon ion density, the aluminum ion density and the aluminum atom density versus time from the pulse initiation. The target was assumed to be made of aluminum 150 mm in diameter, the argon gas pressure was 10 mTorr and the power used was the experimentally determined value shown in Figure 2.

The metal ion flux at the surface takes into account the acceleration of the ions across the presheath $\Gamma_{m+} \approx 0.61 n_{m+} u_{Bm}$, where $u_{Bm}=(k_B T_B/m_{m+})^{1/2}$ is the Bohm velocity for metal ions and $m_{m+}$ is the metal ion mass. The flux of the neutral metal is $\Gamma_m=0.25 n_m v_{th}$. In discharges that are not in thermal equilibrium the electron temperature $T_e$ is typically significantly larger than the neutral gas temperature $T_g$. Thus, the fraction of ionized metal flux at the substrate $\Gamma_{m+}/(\Gamma_m+\Gamma_{m+})$ is larger than the fraction of ionized metal in the plasma $n_{m+}/(n_m+n_{m+})$. The ionized metal fraction and the ionized flux fraction versus time from the pulse initiation is shown in Figure 5. The ionized flux fraction is somewhat higher the fractional ionization of the metal

species. We note that the ionized flux fraction peaks at 0.99 58 $\mu$s after initiating the pulse and the ionization fraction of the metal is 0.88 62 $\mu$s after initiating the pulse. The integrated ionized fraction is 0.76 and the integrated ionized flux fraction is 0.89. So indeed the ionized flux fraction is very high in the high power impulse magnetron sputtering discharge.

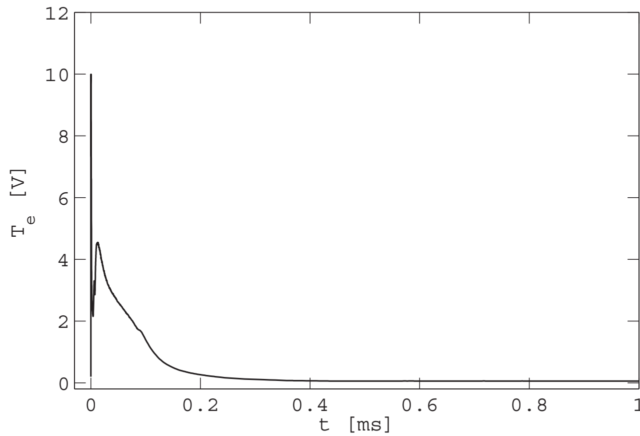

Figure 4: The electron temperature versus time from the pulse initiation. The target was assumed to be made of aluminum 150 mm in diameter, the argon gas pressure was 10 mTorr and the power used was the experimentally determined value shown in Figure 2.

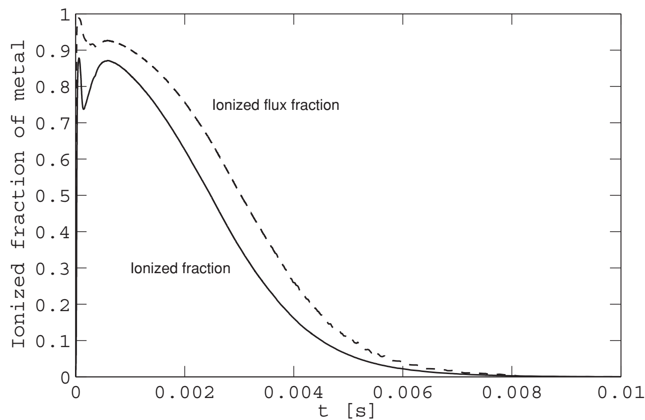

Figure 5: The ionized metal fraction and the ionized flux fraction versus time from the pulse initiation. The target was assumed to be made of aluminum 150 mm in diameter, the argon gas pressure was 10 mTorr and the power used was the experimentally determined value shown in Figure 2.

In Figure 6 we explore the contribution of each of the three processes expected to create metal ions in the pulsed magnetron discharge. We see that during the first 100 $\mu$s from initiating the pulse electron impact ionization is the most effective process in creating metal ions. Charge exchange contributes of the order of 10 - 20% to the creation of metal ions during this period. At about 100 $\mu$s into the pulse charge exchange becomes the dominant process in creating metal ions. Penning ionization is a negligible process in the pulsed discharge.

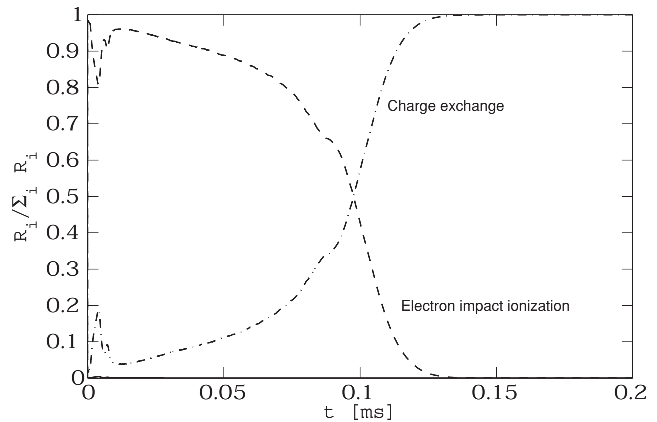

Figure 6: The relative reaction rate versus time from the pulse initiation. The target was assumed to be made of aluminum 150 mm in diameter, the argon gas pressure was 10 mTorr and the power used was the experimentally determined value shown in Figure 2.

## CONCLUSION

The ionization mechanism in high power impulse magnetron sputtering discharge is explored. The ionized metal fraction and the ionized flux fraction are very high and the integrated ionized flux fraction is 0.89 for aluminum. During the first 100 $\mu$s from initiating the pulse (roughly while the pulse is on) electron impact ionization is the most effective process in creating metal ions while charge exchange becomes the dominant process in creating metal ions after the pulse is off. Due to crude assumptions, including Maxwellian electron energy distribution, cross section uncertainties, and in particular spatial uniformity the global model is not meant to give accurate values of the plasma parameters. Experimental work has shown that there is indeed a significant spatial variation in the plasma parameters [11,12]. However, the global model can give an indication of how one parameter depends on another and which reactions among the species are important.

## ACKNOWLEDGEMENTS

The author gratefully acknowledges Prof. Ulf Helmersson at Linköping University Sweden for useful discussions and the Icelandic Research Fund and the University of Iceland Research Fund for financial support during the course of this work

## REFERENCES

1. S.P. Bugaev, N.N. Koval, N.S. Sochugov, and A.N. Zakharov, “Investigation of a high-current pulsed magnetron discharge initiated in the low-pressure diffuse arc plasma”, *Proceedings of the XVIIth International Symposium on Discharges and Electrical Insulation in Vacuum*, pp. 1074-1076 1996

2. V. Kouznetsov, K. Macák, J. M. Schneider, U. Helmersson, and I. Petrov, “A novel pulsed magnetron sputter technique utilizing very high target power densities”, *Surf. Coat. Technol.,* 122, 290, 1999

3. K. Macák, V. Kouznetsov, J. Schneider, U. Helmersson, and I. Petrov , “Ionized sputter deposition using an extremely high plasma density pulsed magnetron discharge”, *J. Vac. Sci. Technol.,* A 18, 1533, 2000

4. U. Helmersson, M. Lattemann, J. Alami, J. Bohlmark, A. P. Ehiasarian, and J. T. Gudmundsson, “High power impulse magnetron sputtering discharges and thin film growth: A brief review”, *48th Annual Technical Conference Proceedings of the Society of Vacuum Coaters*, pp. 458-464, 2005

5. U. Helmersson, M. Lattemann, J. Bohlmark, A. P. Ehiasarian, and J. T. Gudmundsson, “Ionized Physical Vapor Deposition (IPVD): A Review of Technology and Applications”, *Thin Solid Films.,* 513, 1, 2006

6. A. P. Ehiasarian, R. New, W.-D. Münz, L. Hultman, U. Helmersson, and V. Kouznetsov, “Influence of high power densities on the composition of pulsed magnetron plasmas”, *Vacuum,* 65, 147, 2002

7. D. J. Christie, F. Tomasel, W. D. Sproul, and D. C. Carter, “Power supply with arc handling for high peak power magnetron sputtering”, *J. Vac. Sci. Technol.,* A 22, 1415, 2004

8. J. A. Hopwood, “The role of ionized physical vapor deposition in integrated circuit fabrication”, in *Thin Films: Ionized Physical Vapor Deposition*, edited by J. A. Hopwood, Academic Press, San Diego, 2000, pp. 1-7

9. J. A. Hopwood, “Plasma Physics”, in *Thin Films: Ionized Physical Vapor Deposition*, edited by J. A. Hopwood, Academic Press, San Diego, 2000, pp. 181-207

10. J. T. Gudmundsson, J. Alami, and U. Helmersson, “Evolution of the electron energy distribution and plasma parameters in a pulsed magnetron discharge”, *Appl. Phys. Lett.*, 78, 3427, 2001

11. J. Bohlmark, J. T. Gudmundsson, J. Alami, M. Lattemann, and U. Helmersson, “Spatial Electron Density Distribution in a High-Power Pulsed Magnetron Discharge ”, *IEEE Trans. Plasma Sci.*, 33, 346, 2005

12. J. T. Gudmundsson, J. Alami, and U. Helmersson, “Spatial and temporal behavior of the plasma parameters in a pulsed magnetron discharge ”, *Surf. Coat. Technol.*, 161, 249, 2002

13. J. Bohlmark, J. Alami, C. Christou, A.P. Ehiasarian, and U. Helmersson , “Ionization of sputtered metals in high power pulsed magnetron sputtering”, *J. Vac. Sci. Technol.*, A 23, 18, 2005

14. A. P. Ehiasarian, W.-D. Münz, L. Hultman, U. Helmersson, and I. Petrov, “High power pulsed magnetron sputtered $CrN_x$ films ”, *Surf. Coat. Technol.*, 163-164, 267, 2003

15. B. M. DeKoven, P. R. Ward, and R. E. Weiss, D. J. Christie, R. A. Scholl, W. D. Sproul, F. Tomasel, and A. Anders, “Carbon Thin Film Deposition Using High Power Pulsed Magnetron Sputtering ”, *46th Annual Technical Conference Proceedings of the Society of Vacuum Coaters*, pp. 158-165, 2003

16. S. Ashida, C. Lee amd M. A. Lieberman, “Spatially averaged (global) model of time modulated high density argon plasma”, *J. Vac. Sci. Technol.,* A 13, 2498, 1995

17. J. Hopwood and F. Qian , “Mechanisms for highly ionized magnetron sputtering”, *J. Appl. Phys.,* 78, 758, 1995

18. J. T. Gudmundsson, “*Notes on the electron excitation rate coefficients for argon and oxygen discharge*”, Technical Report RH-21-2002, Science Institute, University of Iceland, 2002

19. V. A. Godyak, *Soviet Radio Frequency Discharge Research*, Delphic Associates, Falls Church, V.A., 1986

20. H. C. Straub, P. Renault, B. G. Lindsay, K. A. Smith, and R. F. Stebbings, “Absolute partial and total cross sections for electron-impact ionization of argon from threshold to 1000 eV”, *Phys. Rev. A.*, 52, 1115, 1995

21. K. Tachibana, “Excitation of the 1s5,1s4, 1s3, and 1s2 levels of argon by low-energy electrons”, *Phys. Rev. A.*, 34, 1007, 1986

22. C. Lee and M. A. Lieberman, “Global model of Ar, $O_2$, $Cl_2$, and Ar/$O_2$ high-density plasma discharges”, *J. Vac. Sci. Technol.,* A 13, 368, 1995

23. J. Lu and M. J. Kushner, “Effect of sputter heating in ionized metal physical vapor deposition reactors”, *J. Appl. Phys.,* 87, 7198, 2000

23. D. N. Ruzic, “Fundamentals of Sputtering and Reflection”, in *Handbook of Plasma Processing Technology: Fundamentals, Etching, Deposition, and Surface Engineering*, edited by S. M. Rossnagel, J. Cuomo and W. D. Westwood, Noyes Publications, Park Ridge, New Jersey, 1990, pp. 70-90